J. Inst. Eng. India Ser. C (February 2022) 103(1):29–37
https://doi.org/10.1007/s40032-021-00695-7

ORIGINAL CONTRIBUTION

Finite Element Modeling of Thermal Residual Stresses generated during EDM of AISI 1018 Steel

Saurav Kumar[1] · Sanghamitra Das[2] · Shrikrishna N. Joshi[2]

Received: 18 November 2020 / Accepted: 2 April 2021 / Published online: 23 April 2021

Abstract The spark discharges produced during electric discharge machining (EDM) process results in the generation of a huge amount of temperature and thermal stresses in the workpiece as well as the tool electrode. The thermal residual stresses originated in the workpiece are responsible for abrupt failure of the component due to declining fatigue life. The current study focuses on the prediction of temperature and stresses that are produced during spark discharges on AISI 1018 steel surface with the aid of a finite element model. The model could predict the peak temperature and stresses that are generated on the workpiece surface after EDM cutting. It was further noted that the thermally induced stresses not only affect the workpiece surface but also affected into larger depths with increasing pulse energy. Both compressive and tensile stresses were observed on the machined surface. Minimization of temperature and residual stresses generated during EDM operation by optimizing the input conditions could surely reduce the risk of component failure and lead to better machining efficiency.

Keywords Electrical discharge machining · Thermal residual stresses · Finite element analysis · Electro thermal

List of Symbols

r, z	Cylindrical coordinates of the domain
T	Temperature (K)
T_∞	Ambient temperature (K)
k	Thermal conductivity of the material (W/mK)
ρ	Density of the material (kg/m^3),
q	Heat supplied
t	Time (s)
c_p	Specific heat (J/kgK).
σ_{ij}	Stress tensor
b_i	Body force vector
$d\sigma$, $d\varepsilon$, dT	Stress, strain and temperature increments, respectively
$[D_e]$, $[D_p]$ and $[K_{th}]$	Elastic stiffness matrix, Plastic stiffness matrix and Thermal stiffness matrix, respectively
u_r, u_z	Displacement in r and z directions
F_c	Fraction of total spark energy absorbed by the (cathode) workpiece
V	Discharge voltage (V)
I	Current (A)
t_{on}	Pulse duration (μs)
ζ	Duty factor
R_{pc}	Spark radius (μm)

✉ Shrikrishna N. Joshi
snj@iitg.ac.in

[1] Department of Mechanical Engineering, Dr. APJ Abdul Kalam Technical University, Lucknow, Uttar Pradesh, India

[2] Department of Mechanical Engineering, Indian Institute of Technology Guwahati, Guwahati, India

Introduction

Electrical discharge machining (EDM) is an unconventional machining process to process electrically conductive workpiece irrespective of its hardness and melting point. It is a noncontact process where material removal occurs by the method of melting and vaporization when repetitive spark discharges occur in the interelectrode gap between the electrodes. The wide variety of EDM applications in modern manufacturing operations like machining of dies, automobile parts, biomedical industries, etc. make the process extremely useful. The generation of plasma due to the sparks produced raises the temperature of the machining zone considerably. This high temperature originates thermal and residual stresses on the workpiece surface which might initiate the onset of component failure. Thermally generated stresses degrade the workpiece quality and integrity leading to microcrack formation on the surface. These microcracks might propagate into deeper cracks finally causing failure of the EDMed product.

The literature reports a number of studies to estimate the thermally induced stresses that are produced on the workpiece surface due to extreme rise in temperature during the spark discharges. These stresses are responsible for fatigue failure of the machined components. Das et al. [1] predicted the temperature isotherm and stress profile in the workpiece after EDM cutting of L6 tool steel. Yadav et al. [2] developed a finite element model (FEM) to evaluate the effect of thermal stresses during EDM processing of HSS material. Thermal stresses exceeded the yield stress of the material in the heat affected region. An analytical model was demonstrated by Panda [3] to compute thermal stress components and concluded that pulse duration and discharge current are the most crucial parameters for the thermal damage in EDM. Allen and Chen [4] validated the formation of microcracks on the workpiece surface due to tensile residual stresses generated after successive and random discharges. Thermal and residual stresses formed on the component surface and the plastic strains produced after the yielding point have been evaluated for different steels at different cooling rates [5]. Mamalis et al. [6] measured the residual stresses which were found to be very close to the ultimate strength of the material during EDM of micro-alloyed steel by the *X*-ray diffraction technique. The effects of various input conditions on the residual stresses produced during cutting of D2 steel were observed by Mohanty et al. [7]. Shabgard et al. [8] established that the temperature-induced stresses that are originated on the workpiece surface after the discharge cycle are tensile in nature, which exceeded the ultimate stress of the material. The upper limit of residual stress values is located in a region near the interaction of recast layer and irradiated region of the workpiece [9]. Salvati and Korsunsky [10] further measured the residual stresses produced on the surface of AA6082–T6 aluminum material and compared the results with a FEM model. The role of residual stresses in the crack propagation and breakage of wire electrode during WEDM operation was demonstrated by Das and Joshi [11]. Wu et al. [12] developed a FEM model to estimate the generation of residual stress and phase transformation in Ti–6Al-4 V alloy during WEDM operation. The residual stresses retained in P91 steel after WEDM cutting were found to be tensile in nature, which reduced the fatigue strength of the workpiece [13]. Zhang et al. [14, 15] studied the influence of thermal residual stresses produced due to steep temperature gradients on the deformation of WEDMed thin walled components. Guu et al. [16] observed the formation of microcracks, voids and pits on the machined surface due to tensile residual stresses produced during spark generation. Ekmekci et al. [17] used the *X*-ray diffraction technique to measure the amount of stresses retained in the workpiece after machining and observed the effects of dielectric fluid and tool material on the formation of white layer. Thermal residual stresses are one of the main factors responsible for the formation of microcracks on the machined surface [18]. Navas et al. [19] concluded that the thermal residual stresses generated during WEDM cause serious damage to the component as compared to hard turning and grinding.

Thus, evaluation of thermally induced stresses in EDMed components is very important in order to maintain the surface quality and integrity of the products. The residual stresses retained should be at a minimum level to avoid sudden failure of the parts. In the current study, a two-dimensional electrothermal FEM model has been developed for AISI 1018 steel to compute the temperature and stresses induced during a single pulse cycle. Gaussian heat flux has been incorporated in the model, which is considered as a more realistic approach compared to previous models. The influence of input conditions, viz., discharge current (I), discharge duration (t_{on}) and duty cycle (ζ) on the temperature obtained, and the induced stresses in the workpiece have been studied in detail.

Development of Electrothermal Model

A two-dimensional electrothermal FEM model has been developed for a single pulse cycle to calculate the temperature and thermal residual stresses induced in the workpiece using a commercial FEM software, ANSYS. Figure 1 illustrates the schematic for the developed electrothermal model.

The temperature predicted by the model is specified as input condition to the structural model to compute the

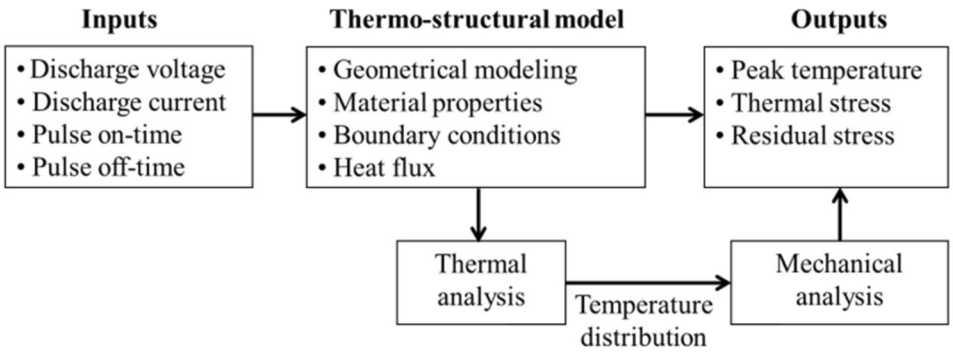

Fig. 1 Schematic of the electrothermal FEM model

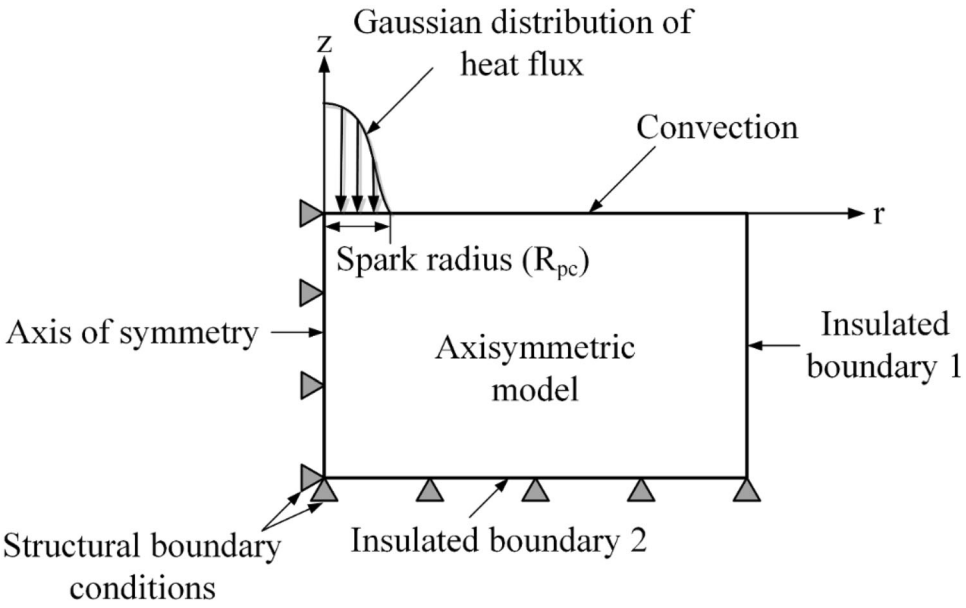

Fig. 2 Process continuum of the two-dimensional axisymmetric model

stresses generated due to temperature increase. An axisymmetric two-dimensional continuum is considered for analysis which is shown in Fig. 2.

Assumptions

- Workpiece is considered to be homogeneous and isotropic.
- The model is considered to be two-dimensional axisymmetric.
- The workpiece surface is free from residual stresses before EDM cutting.
- Gaussian distribution of heat flux.
- The spark radius is dependent on discharge current and time.
- The model is developed for a single spark.
- Plasma flushing efficiency is 100%.
- Only a portion of heat flux is dissipated into the workpiece. The rest of the heat is absorbed by the tool and carried away by the dielectric fluid.

Governing Equations

The two-dimensional partial heat differential conduction equation is considered as the governing equation for the thermal analysis which is given as,

$$\frac{1}{r}\frac{\partial}{\partial r}\left(k\,r\,\frac{\partial T}{\partial r}\right) + \frac{\partial}{\partial z}\left(k\frac{\partial T}{\partial z}\right) + q = \rho c_p \frac{\partial T}{\partial t} \tag{1}$$

The temperature was estimated initially by the model which was given as input to the structural analysis to estimate the thermally induced stresses generated on the workpiece surface.

The governing equations employed for the structural analysis is given as,

$$\sigma_{ij} + \rho\, b_i = 0, \quad \sigma_{ij} = \sigma_{ji} \tag{2}$$

$$[d\sigma] = ([D^e] + [D^p])\,[d\varepsilon] + [K^{\text{th}}]\,dT \tag{3}$$

Boundary Conditions

For thermal analysis, the incorporated boundary conditions are given as,

$$k\frac{\partial T}{\partial z} = \begin{Bmatrix} h(T - T_\infty) \text{ if } r > R_{pc} \\ q \text{ if } r \le R_{pc} \\ 0 \text{ for off-time} \end{Bmatrix} \quad (4)$$

For structural analysis, the incorporated boundary conditions are given as,

$$\begin{matrix} u_r = 0,\ u_z \neq 0, & \text{for axis of symmetry} \\ u_r \neq 0,\ u_z = 0, & \text{for boundary 2} \end{matrix} . \quad (5)$$

The thermal and structural boundary conditions are depicted in Fig. 2. The initial temperature at time $t = 0$ is considered to be at room temperature of 300 K.

Spark Radius

A single spark radius is very difficult to determine experimentally due to the short duration of pulses. Thus, an empirical spark radius equation (Eq. 6) established by Ikai and Hasiguchi [20] has been used in the present model as suggested by previous researchers [21].

$$R_{\text{pc}}\,(\mu m) = 2.04 \times 10^{-3} \times I^{0.43} \times t_{\text{on}}^{0.44} \quad (6)$$

Heat Flux

There have been various efforts to model the EDM process by using different heat flux shapes and predict different shapes of a crater experimentally such as hemispherical, cuboidal and disk shaped. Snoeys and Van Dijck [22] modeled the EDM process as a semi-infinite cylinder heated with a disk input heat source. Beck [23] approached in a similar manner considering constant thermal properties and heat flux. Later, Dibitonto et al. [24] employed the Point heat source model for cathode erosion during EDM which predicted better accuracy in results as compared to the previous models. Joshi and Pande [21] experimentally obtained that the crater formed during single spark experiments is bowl shaped and not uniform. Hence, the heat flux distribution was considered to be bell shaped instead of point heat source or disk-shaped heat source. Gaussian heat flux was employed to predict the material removal rate during EDM operation by considering more realistic features like latent heat of the material, current and pulse on-time dependent spark radius equation. The results predicted by this model showed close approximation with the experimentally obtained results and hence was followed by future researchers. The Gaussian distribution of heat flux for an EDM spark is represented as given in Eq. 7 [21].

$$q(r) = \frac{4.57 F_{\text{c}}\, V\, I}{\pi R_{\text{pc}}^2} \exp\left\{-4.5\left(\frac{r}{R_{\text{pc}}}\right)^2\right\} \quad (7)$$

In the present FEM model, the value of F_c is assumed as 0.183 as suggested by Dibitonto et al. [24].

Solution Methodology

The heat conduction equation and the stress analysis equation are solved by utilizing the FEM method by incorporating the boundary conditions to predict the temperature and thermally generated stresses produced at the end of a single EDM spark. A two-dimensional process continuum was considered for analysis. The process model was solved with the aid of a commercial FEM software ANSYS parametric design language (APDL). The element PLANE 35 was selected for meshing operation, and the mesh size was refined to 5 μm at the location where spark was applied. The mesh size was refined to achieve accurate and better convergence of results. Figure 3 depicts the meshed model of the workpiece along with the boundary conditions. Heat flux is applied in the spark radius region and convection is applied outside the spark region of boundary 1. The convective heat transfer coefficient is considered as 10,000 W/m^{2}K.

In the present work, AISI 1018 steel has been considered as the workpiece material for the developed model to compute the temperature and stresses generated during EDM sparks. The material properties of AISI 1018 steel are listed in Table 1.

In the present model, the gap voltage was kept constant at 40 V based on the previous literature and after carrying out trial experiments based on the facilities available in the central workshop of our institute. Trial experiments were first carried out at varying voltages, viz., 20 V, 30 V, 40 V, 50 V, and it was observed that stable spark discharges without arcing were obtained at a gap voltage of 40 V. Hence, this value was chosen for the present analysis. The effects of three machining conditions, viz., discharge current, discharge duration and duty cycle on the response variables, were studied at three different levels. Table 2 shows the input conditions considered and their chosen levels. The process parameters have been selected by performing extensive preliminary experiments. The trade literature and research articles have been duly referred to choose the ranges of the input parameters.

Results and Discussion

In the current study, three process parameters were considered varied at three different levels. According to the three-level full factorial design, a total of 3^k sets are considered for analysis, where k is the number of factors varied at three different levels. Based on this theory, a total of $3^3 = 27$ simulations have been carried out to investigate the effects of process conditions on the temperature obtained and the thermal residual stresses generated during the EDM process. Figure 4a shows the temperature isotherm after a

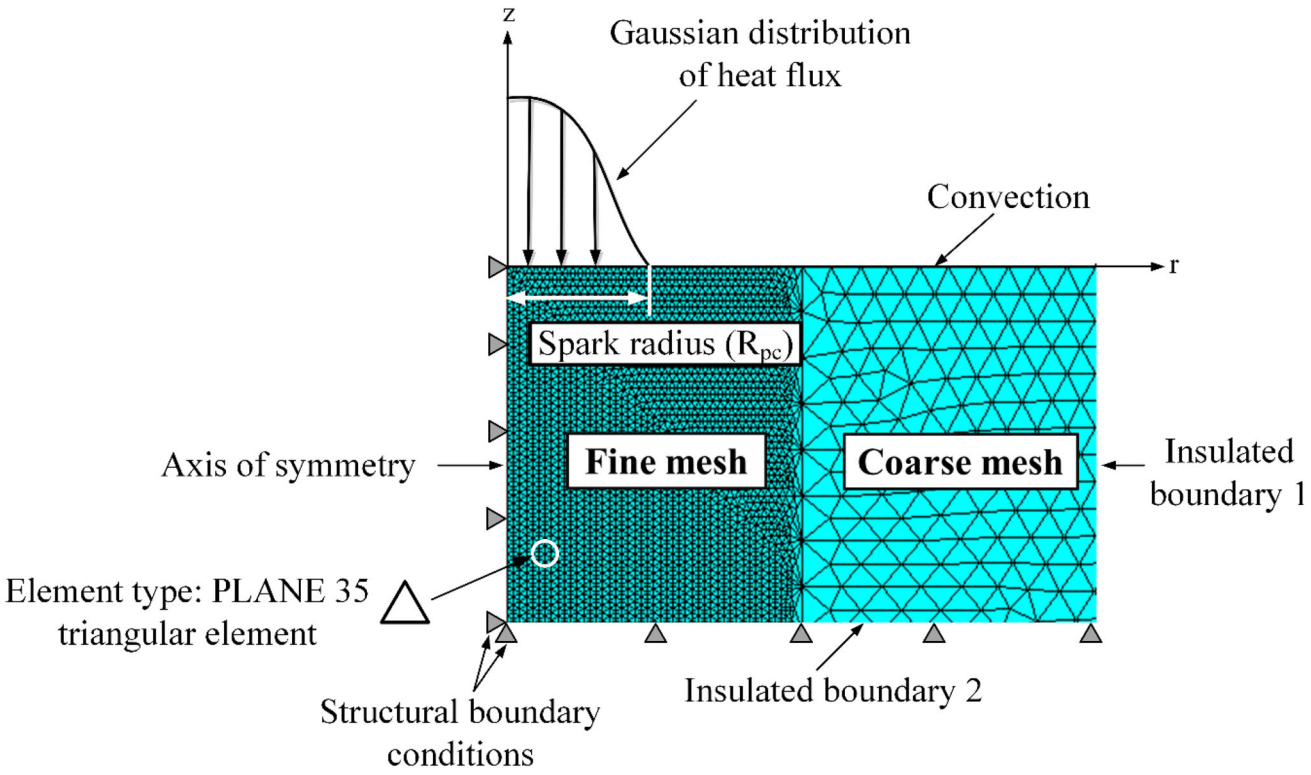

Fig. 3 Meshed process domain

Table 1 Material properties of AISI 1018 steel [25]

Properties	Values
Thermal conductivity (W/mK)	51.9
Specific heat (J/kgK)	486
Density (kg/m^3)	870
Coefficient of thermal expansion (K^{-1})	11.2×10^{-6}
Melting point (K)	1850
Young's modulus (N/m^2)	2×10^{11}
Poisson's ratio	0.29

Table 2 Selected levels of process parameters

Factors	Level 1	Level 2	Level 3
I (A)	4	12	24
t_{on} (μs)	50	100	200
ζ (%)	50	65	80

single spark at the process condition: V = 40 V, I = 4 A, t_{on} = 50 μs, ζ = 50%. The peak temperature obtained is around 6836 K which exceeds the melting point of AISI 1018 steel. The elements in the model, which attained temperature higher than the melting point of the workpiece material, are removed by the ELEMENT KILL method in ANSYS.

The non-uniform temperature distribution during EDM operation causes the formation of thermal and residual stresses in the workpiece, which degrades the quality of the product. The residual stress induced should be low to avoid defects such as formation of microcracks, voids, decrease of fatigue life and finally failure of the component. Figure 4b shows the stress contour induced after a single pulse.

Figure 4b shows that a maximum stress of about 188 MPa is obtained. The equivalent stress decreases along the axial as well as radial directions gradually. This trend of variation seems to be in line with the results reported by previous authors [2]. In order to validate the results of the developed FEM model, the predicted residual stress contour on the workpiece surface are compared with the already published results of Yadav et al. [2], Panda [3] and the experimental results reported by Ekmekci et al. [26]. The results were compared which showed that the residual stress values predicted by our model are well in agreement with published data (Table 3). Figure 5 shows the stress profile variation along the radial and depth direction in the workpiece.

It is noted from Fig. 5(a) that residual stresses are compressive in nature in the vicinity of the spark location (r = 0). The compressive residual stresses rise due to the fact that, with increase in temperature, material tries to expand but gets restrained by the surrounding material.

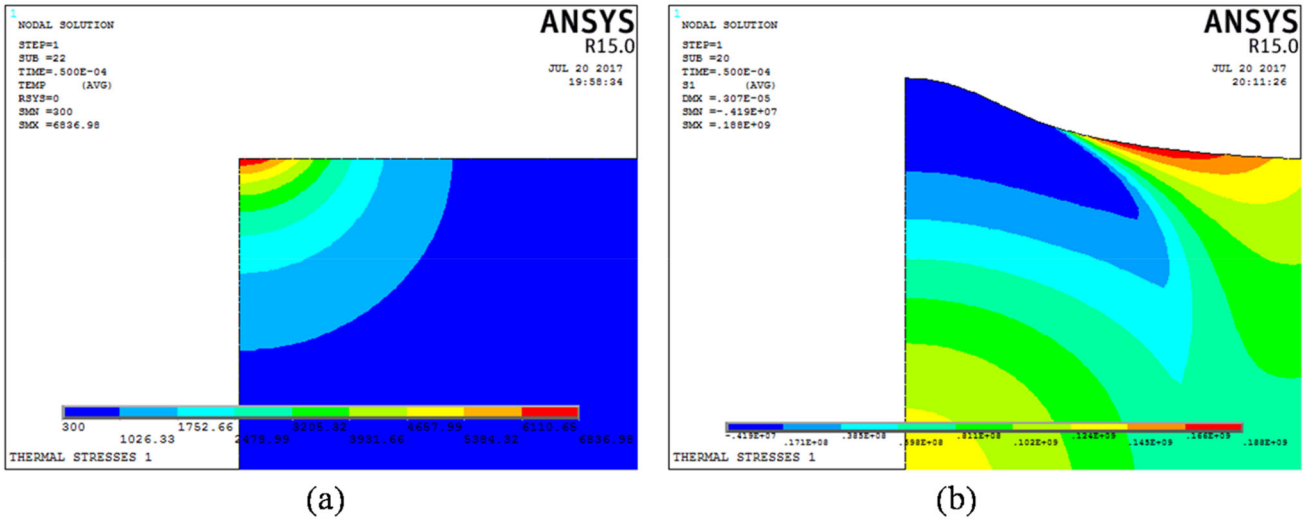

Fig. 4 **a** Temperature contour plot after a single EDM pulse **b** Stress contour induced after a single EDM pulse

Table 3 Comparison of the predicted results: Residual stress along the radial direction

Published report	I (A)	t_{on} (μs)	ζ (%)	Our numerical model (MPa)	Published data (MPa)	Absolute deviation (%)
Panda [3]	12	100	65	− 200 (at a radial distance of 400 μm)	− 193.76 (at a radial distance of 400 μm)	3.22

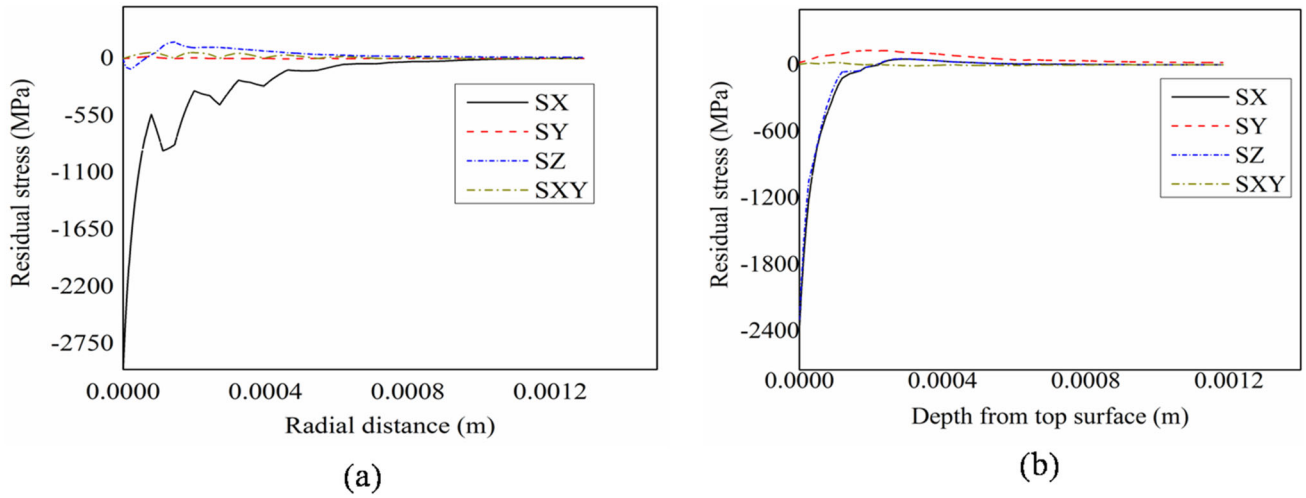

Fig. 5 Residual stress variation along the **a** radial direction **b** depth

Further, it was noticed that the stress component along the radial direction (SX) has the highest magnitude and gradient as compared to stress values along other directions and hence was dominant in nature. At a certain radial distance, the magnitude of residual stress is found to exceed the ultimate tensile strength of AISI 1018 material, which might cause the initiation of cracks near the surface. There is approximately no stress formation beyond 900 μm away from the center. Figure 5b represents the thermal residual stress contour beneath the top surface of the workpiece along the depth direction. It is noticed that almost all the stress components are found to be compressive in nature followed by tensile nature. This tensile stress is due to the presence of white layer which is found in the recast zone of the affected area. Stresses vary up to 300 μm and no stresses are found beyond 900 μm of depth. The most critical components of stress are the radial stress component (SX) and the longitudinal stress component (SZ) which varies from –2250 MPa to + 75 MPa within 400 μm of depth. This indicates that SX and SZ

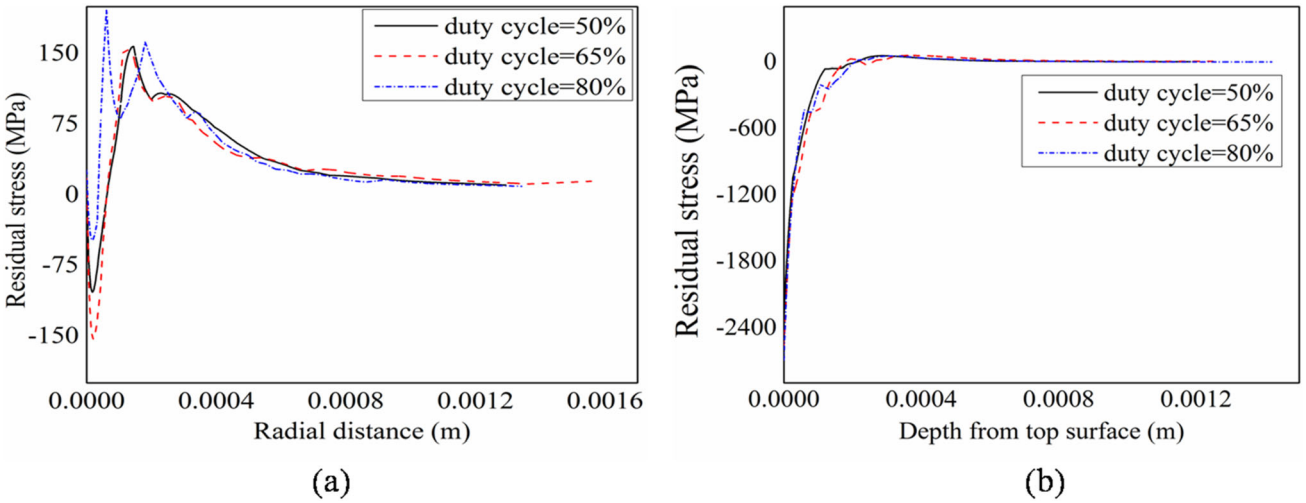

Fig. 6 Residual stress variation with duty cycle along the **a** radial direction **b** depth

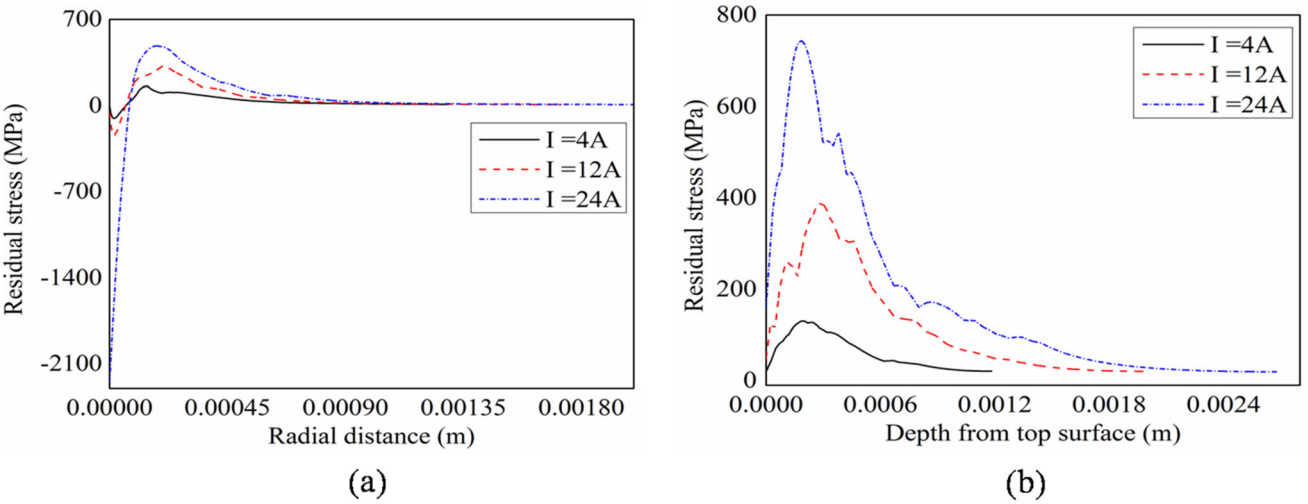

Fig. 7 Residual stress variation with current along the **a** radial direction **b** depth

components will generate more stresses near the surface. It has also been observed that the radial, tangential, longitudinal and shear stress components and their distribution show similar trend and nature with the results reported by Yadav et al. [2].

Effects of Process Parameters on Residual Stress Distribution

In order to examine the influence of machining conditions on the residual stresses retained in the workpiece after a single pulse, parametric studies were performed. Figures 6 and 7 show the influence of duty cycle and current, respectively, on the variation of residual stresses in both the radial and depth direction.

The graphs clearly depict that the radial and longitudinal stress components increase with the rise in duty cycle values. The reason behind this is that larger heat is dissipated at higher values of duty cycle, which increases the peak temperature obtained during the spark discharges. The radial stress components vary up to a distance of 500 µm, whereas variation in longitudinal stress components is found up to 600 µm. Also it is quite interesting to note that residual stress along the radial direction changes its sign from negative to positive within 600 µm. This can be explained by the presence of small martensite (white) layer below, which expands during cooling, causing extra tensile stresses in the surrounding material. It is further observed from Fig. 6b that residual stress variation with duty cycle is less significant along the depth. The stress

profiles shown in the above figures also show a similar trend of stress variation with the results reported by Yadav et al. [2].

Figure 7 shows that on increasing the pulse current, the induced residual stress components also increase. The increase in temperature due to increase in pulse current results in higher thermally induced stresses which might cause the origination of cracks on the workpiece surface. Moreover, on increasing the pulse current, white layer thickness also increases, which leads to increased tensile stress [27]. This causes the formation of cracks on the EDMed surface. It is interesting to note from Fig. 7a that residual stress changes its nature from compressive to tensile within 750 μm and beyond that it becomes zero. Figure 7b shows that the residual stress components increase in the same rate as that of rise in pulse current. It has been further concluded that the residual stress contour obtained in the workpiece is independent of discharge energy settings. However, the width of the peak residual stress changes with the variation in spark energy.

Conclusions

Steep temperature gradients generated during spark discharges in EDM process causes thermal and residual stresses in the irradiated region which affects the integrity and fracture strength of the components. Thus, prediction and estimation of residual stresses retained in the part is of utmost importance in order to prevent failure of the component. In the present work, a two-dimensional electrothermal model is developed for AISI 1018 steel to evaluate the temperature rise and residual stresses produced during a single pulse discharge. The results estimated by the FEM model are well validated with the published results and are observed to be in close agreement. The results indicate that the temperature rises during the pulse on-time, and then, it decreases rapidly during the pulse off-time. It has been observed that the compressive residual stresses are generated below the surface and the tensile residual stresses are created away from the irradiated region. Parametric studies have been performed which shows that induced stresses increase with the rise of current due to increase in heat flux supplied. It is also concluded that the values of radial and longitudinal stress components increase with larger duty cycle values. However, with the increase in pulse duration the maximum thermal load decreases which also reduces the peak values of stresses induced in the workpiece.

Acknowledgements This paper is a revised and expanded version of an article entitled, 'Thermal residual stress analysis during electrical discharge machining of AISI 1018 steel' presented in '7th International Conference on Advancements and Futuristic Trends in Mechanical and Materials Engineering' held at Indian Institute of Technology Ropar, Roopnagar, India during December 5-7, 2019.

Declarations

Conflict of interest No conflict of interest.

References

1. S. Das, M. Klotz, F. Klocke, J. Mater. Process Technol. **142**, 2 (2003). https://doi.org/10.1016/S0924-0136(03)00624-1
2. V. Yadav, V.K. Jain, P.M. Dixit, Int. J. Mach. Tools Manuf. **42**, 877 (2002). https://doi.org/10.1016/S0890-6955(02)00029-9
3. D.K. Panda, J. Mater. Process Technol. **202**, 86 (2008). https://doi.org/10.1016/j.jmatprotec.2007.09.040
4. P. Allen, X. Chen, J. Mater. Process Technol. **186**, 346 (2007). https://doi.org/10.1016/j.jmatprotec.2007.01.009
5. J.O. Kristiansson, J. Therm. Stresses **5**, 315 (1982)
6. A.G. Mamalis, G.C. Vosniakos, N.M. Vacevanidis, X. Junzhe, CIRP Ann. **37**(1), 531–535 (1988). https://doi.org/10.1016/S0007-8506(07)61694-1
7. C.P. Mohanty, J. Sahu, S.S. Mahapatra, Procedia Eng. **51**, 508 (2013). https://doi.org/10.1016/j.proeng.2013.01.072
8. M. Shabgard, S. Seydi, M. Seyedzavvar, Int. J. Adv. Manuf. Technol. **82**, 1805 (2016). https://doi.org/10.1007/s00170-015-7510-7
9. J. Tang, X. Yang, J. Phys. D: Appl. Phys. **51**, 135308 (2018). https://doi.org/10.1088/1361-6463/aab1a8
10. E. Salvati, A.M. Korsunsky, J. Mater. Process Technol. **275**, 116373 (2020). https://doi.org/10.1016/j.jmatprotec.2019.116373
11. S. Das, S.N. Joshi, J. Manuf. Process. **53**, 406 (2020). https://doi.org/10.1016/j.jmapro.2020.03.015
12. H. Wu, J. Ma, Q. Meng, M.P. Jahan, F. Alavi, Procedia Manuf. **26**, 359 (2018). https://doi.org/10.1016/j.promfg.2018.07.044
13. S. Bhattacharya, A. Mishra, T. Singh, S. Bandyopadhyay, S. Kumar, G.K. Dey, V. Kain, Mater. Today Proc. **19**, 462 (2019). https://doi.org/10.1016/j.matpr.2019.07.636
14. Y. Zhang, S. Guo, Z. Zhang, H. Huang, W. Li, G. Zhang, Y. Huang, J. Mater. Process. Technol. **270**, 306 (2019). https://doi.org/10.1016/j.jmatprotec.2019.02.020
15. Y. Zhang, Z. Zhang, H. Huang, Y. Huang, G. Zhang, W. Li, C. Liu, J. Manuf. Process. **31**, 9 (2018). https://doi.org/10.1016/j.jmapro.2017.10.024
16. Y.H. Guu, H. Hocheng, C.Y. Chou, C.S. Deng, Mater. Sci. Eng. A **358**, 37 (2003). https://doi.org/10.1016/S0921-5093(03)00272-7
17. B. Ekmekci, Appl. Surf. Sci. **253**, 9234 (2007). https://doi.org/10.1016/j.apsusc.2007.05.078
18. P. Govindan, S.S. Joshi, J. Manuf. Process. **14**, 277 (2012). https://doi.org/10.1016/j.jmapro.2012.05.003
19 V.G. Navas, I. Ferreres, J.A. Marañón, C. Garcia-Rosales, J.G. Sevillano, J. Mater. Process. Technol. **195**, 186 (2008). https://doi.org/10.1016/j.jmatprotec.2007.04.131
20. T. Ikai, K. Hashigushi, In Proceedings of international symposium for electro-machining-ISEM XI. EPFL, Switzerland, (1995).
21. S.N. Joshi, S.S. Pande, J. Manuf. Process. **12**, 45 (2010). https://doi.org/10.1016/j.jmapro.2010.02.001
22. R. Snoeys, F.S. Van Dijck, CIRPI Ann.—Manuf. Technol. **20**, 35–36 (1971)
23. J.V. Beck, Int. J. Heat Mass Transf. **24**, 1631 (1981). https://doi.org/10.1016/0017-9310(81)90071-5
24. D.D. DiBitonto, P.T. Eubank, M.R. Patel, M.A. Barrufet, J. Appl. Phys. **66**, 4095 (1989). https://doi.org/10.1063/1.343994
25. S.N. Joshi, S.D. Pande, AIP Conf. Proc. **1353**, 1373 (2011)

26. B. Ekmekci, A.E. Tekkaya, A. Erden, Int. J. Mach. Tools Manuf. **46**, 858 (2006). https://doi.org/10.1016/j.ijmachtools.2005.07.020
27. H.T. Lee, T.Y. Tai, J. Mater. Process Technol. **142**, 676 (2003). https://doi.org/10.1016/S0924-0136(03)00688-5